Materials Chemistry and Physics 136 (2012) 247–253

Contents lists available at SciVerse ScienceDirect

Materials Chemistry and Physics

journal homepage: www.elsevier.com/locate/matchemphys

Transparent polyimide/graphene oxide nanocomposite with improved moisture barrier property

I-Hsiang Tseng, Yu-Fu Liao, Jen-Chi Chiang, Mei-Hui Tsai*

Department of Chemical and Materials Engineering, National Chin-Yi University of Technology, No. 57, Sec. 2, Zhongshan Rd., Taipin Dist., Taichung 41170, Taiwan

HIGHLIGHTS

- Colorless and organo-soluble PI was synthesized via one-step process.
- Blending graphene oxide with PI in DMAc enhances gas barrier property of PI.
- PI/GO nanocomposite exhibits excellent moisture resistance and optical clarity.
- Homogeneous distribution of GO in PI leads to low CTE and low WVTR.

GRAPHICAL ABSTRACT

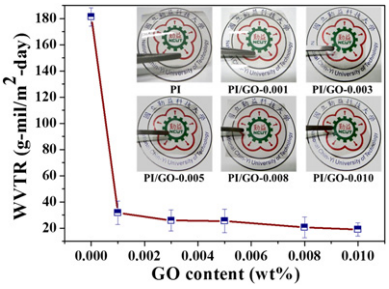

ARTICLE INFO

Article history:
Received 23 December 2011
Received in revised form
14 June 2012
Accepted 26 June 2012

Keywords:
Nanostructures
Polymers
Optical properties
Transport properties

ABSTRACT

Colorless and organo-soluble polyimide (PI) films have been synthesized from an alicyclic dianhydride BCDA and aromatic diamine 3,4′-ODA in the cosolvent of DMAc and GBL via one-step process. The graphene oxide (GO) was mixed with the above PI in DMAc solution to fabricate the PI/GO nanocomposite films. With the addition of only 0.001 wt% of GO in PI matrix, the resultant nanocomposite (PI/GO-0.001) exhibits not only the enhanced resistance to moisture but also retains superior visible light transmission, enhanced mechanical strength, and excellent dimensional stability, simultaneously. The water-vapor-transmission-rate (WVTR) significantly reduced to 30 g mil m^{-2} day^{-1} for this nanocomposite compared to 181 g mil m^{-2} day^{-1} for pure PI. Notably, the PI/GO-0.001 nanocomposite also exhibits low coefficient of thermal expansion (CTE) of 41 ppm $°C^{-1}$, which is benefited from the homogeneous distribution of ultrathin GO nanosheets in PI matrix.

1. Introduction

Aromatic polyimides (PIs) exhibit excellent mechanical and thermal properties that they are promising materials for substrates or interlayers in advanced semiconductors and microelectronics industries. However, those PIs with their excellent high-temperature stability exhibit poor solvent solubility, hence limiting their processability. In addition, the highly conjugated aromatic structure causes the formation of intermolecular charge–transfer complex in PI matrix, leading to the yellowish coloration [1–6]. Optical transparency and/or organo-solubility of PIs can be enhanced by introducing alicyclic or noncoplanar structures, pendant bulky groups or flexible bridging units into the backbone of PIs [5–8]. However, such modifications usually sacrifice the thermal and/or mechanical properties of PI. Another method to synthesize colorless PI is to introduce the inorganic moiety, such as silica and clay, into the PI matrix [9–18]. It was found that the mechanical, thermal and anticorrosive properties of colorless PI films were significantly improved by the incorporation of a small amount of those nanofillers. Moreover, the introduction of layered clay materials in PI matrix reduces the gas permeability rate [16–18] probably due to their high aspect ratio and having good alignment in polymer matrix [19].

* Corresponding author. Tel.: +886 4 23924505; fax: +886 4 23926617.
E-mail address: tsaimh@ncut.edu.tw (M.-H. Tsai).

0254-0584/$ – see front matter © 2012 Elsevier B.V. All rights reserved.
http://dx.doi.org/10.1016/j.matchemphys.2012.06.061

Recently, layered graphene has attracted tremendous attention due to its extraordinary electronic and mechanical properties [20–24]. In addition, graphene and graphene-derived layered materials are also considered as potential candidates of gas barrier membranes [19,24–28]. For example, a monolayer graphene layer was found impermeable to He, Ar and air [24]. The polystyrene nanocomposites containing crumpled graphene nanosheet show better enhanced oxygen barrier property than those containing commonly used clay [19]. The graphene platelets were excellent diffusion barriers that the N_2 or O_2 permeation can be remarkably reduced in polyurethane or poly(vinyl alcohol) nanocomposites [27,28]. Polymer films with improved gas or moisture barrier capability are widely used in various applications such as food packaging and advanced microelectronic device [27–32]. To date, the experimental measurement of water barrier ability of graphene-based nanofiller in polyimide matrix is still lack in literature.

In this study, graphene oxide (GO), which can be produced from inexpensive graphite powder by Hummers method and followed by exfoliation [25,26,33–36], was selected as the nanofiller to blend with organo-soluble PI based on the alicyclic dianhydride and aromatic diamine in cosolvent. The objective of this study is to evaluate the effects of GO content on the water-vapor-transmission-rate (WVTR) and the optical transparency of synthesized colorless PI/GO nanocomposites. The thermal and mechanical properties of obtained PI/GO nanocomposites were also examined. The results suggest that GO nanosheets form a good gas barrier in PI matrix and thus reduce the moisture permeation though PI nanocomposite films. In addition, the obtained colorless PI nanocomposites remain excellent optical clarity and favorable thermal stability as well as have enhanced mechanical strength and dimensional stability.

2. Experimental

2.1. Materials

Bicyclo[2.2.2]oct-7-ene-2,3,5,6-tetracarboxylic dianhydride (BCDA) and 3,4′-oxydianiline (ODA) purchased from Aldrich were used as-received. γ-Butyrolactone (GBL) and dimethylacetamide (DMAc) were provided by TEDIA. The catalyst, isoquinoline and HCl (37%), H_2SO_4 (98%), H_2O_2(30%), $KMnO_4$ were commercially obtained from TCI. Graphite powder (325 mesh) was supplied by Alfa-Aesar.

2.2. Synthesis of transparent PI solution

Organo-soluble PI with solid content of 20w% was synthesized from the reaction of equal molar BCDA and ODA in cosolvent via one-step method. A typical batch containing ODA (3.5526 g) and BCDA (4.4474 g) was completely dissolved in the cosolvent (GBL and DMAc, 16 g) and continuously mixed by a mechanical stirrer at room temperature under N_2. After 2 h, the isoquinoline was mixed with the above poly(amic acid) (PAA) solution and continuously stirred at 170–180 °C for 12–15 h to complete the imidization process. The resultant viscous, transparent and pale yellow PI solution was cooled and slowly decanted into excess methanol to solidify PI. The PI precipitate was washed by continuously stirring in methanol in order to remove unreacted monomers or low-molecular-weight PI. After drying in a vacuum oven at 150 °C, the collected PI precipitate can be easily stored or dissolved in DMAc for further casting pure PI films or preparing PI/GO hybrids.

2.3. Preparation of GO nanosheets

A modified Hummers method was utilized to synthesize GO powder. The natural graphite (3 g) was mixed with $NaNO_3$ (3 g) and concentrated H_2SO_4 (50 mL) in a 250 mL three-neck flask in an ice bath, and followed by the slow addition of 15 g of $KMnO_4$. The mixture was continuously stirred for 48 h and then H_2O_2 (35 mL) was slowly added into the mixture. The fully oxidized suspension was poured into a large amount of distilled water. The solid products were obtained after filtration and washing process with 10% HCl solution to achieve a pH value higher than 6. The GO powder was obtained after drying at 60 °C in a vacuum oven.

2.4. Preparation of PI/GO nanocomposites

PI/GO nanocomposites with various loadings of GO were synthesized by the following procedure shown in Scheme 1. The dried PI precipitate (1.5 g) was completely dissolved in DMAc to obtain PI solution with the solid content of 20 wt% at ambient condition. For preparing PI containing 0.001wt% of GO, GO (0.0015 g) suspended in DMAc (2 g) was ultrasonicated for at least 2 h and then mixed with the above PI solution. The degassed PI/GO solution was casted on a clean glass substrate by a doctor-blade and cured at elevated temperatures. A reference pure PI sample was also casted by using the pure PI solution. All the casted films were thermally imidized via the following program to complete the imidization process: at a rate of 0.3–0.6 °C min^{-1} to 100 °C, 140 °C, 160 °C and 180 °C, isothermal at each temperature for 1 h, and finally to 210 °C for 5 h. The sample code is denoted PI–GO-*x*, where *x* indicates the weight percentage of GO in final hybrid film.

2.5. Characterization

X-ray diffraction (XRD) experiments were conducted on an X-ray diffractometer (PANalytical X'Pert PRO) using Cu Kα radiation ($\lambda = 0.154$ nm) at an accelerating voltage of 40 kV and current of 30 mA. Scanning electron microscope (SEM, Tescan) was performed at an acceleration voltage of 3 kV to observe the morphology of fractured surfaces of samples. Infrared spectra of the PI solution at various temperatures were obtained by using a Nicolet Protégé-460 Fourier transform infrared (FTIR) spectrophotometer equipped with a variable-temperature sample holder. The PI solution was spin-coated on KBr and heated at a rate of 20 °C min^{-1} to a specific temperature (*T*). After isothermal for 5 min, the IR spectrum was conducted. The optical properties, including transmittance, haze and L^*, a^*, b^* values of spin-coated thin films were examined by a UV–Vis/Color spectrophotometer (HUNTERLAB, Ultrascan VIS). The water-vapor-transmission-rate (WVTR) of each sample with the size of 20 cm^2 was measured using a permeation test system (MOCON, Permatran-W 3/61) at atmospheric pressure, 40 °C and 100% relative humidity. The dynamic mechanical analysis (DMA) was performed with a Dupont DMA-2980 at a frequency of 1 Hz, from 60 to 350 °C and at a heating rate of 3 °C min^{-1}. Thermogravimetric analysis (TGA) was carried out with a TGA-Q500 from TA Instrument at a heating rate of 20 °C min^{-1} under nitrogen. The thermal mechanical analyzer (TMA, TA Instrument, Q-400) was conducted under an extension mode, with a tension force of 0.05 N, at a heating rate of 10 °C min^{-1}, at a frequency of 1 Hz and under nitrogen. The coefficient of thermal expansion (CTE) was determined by the dimension change in the temperature range of 100–200 °C, which is the commonly applied testing condition in manufacturers.

3. Results and discussion

3.1. Characteristics of GO

The morphology and XRD pattern of obtained GO were displayed in Fig. 1. The ultra thin sheets with wrinkled and silk-like

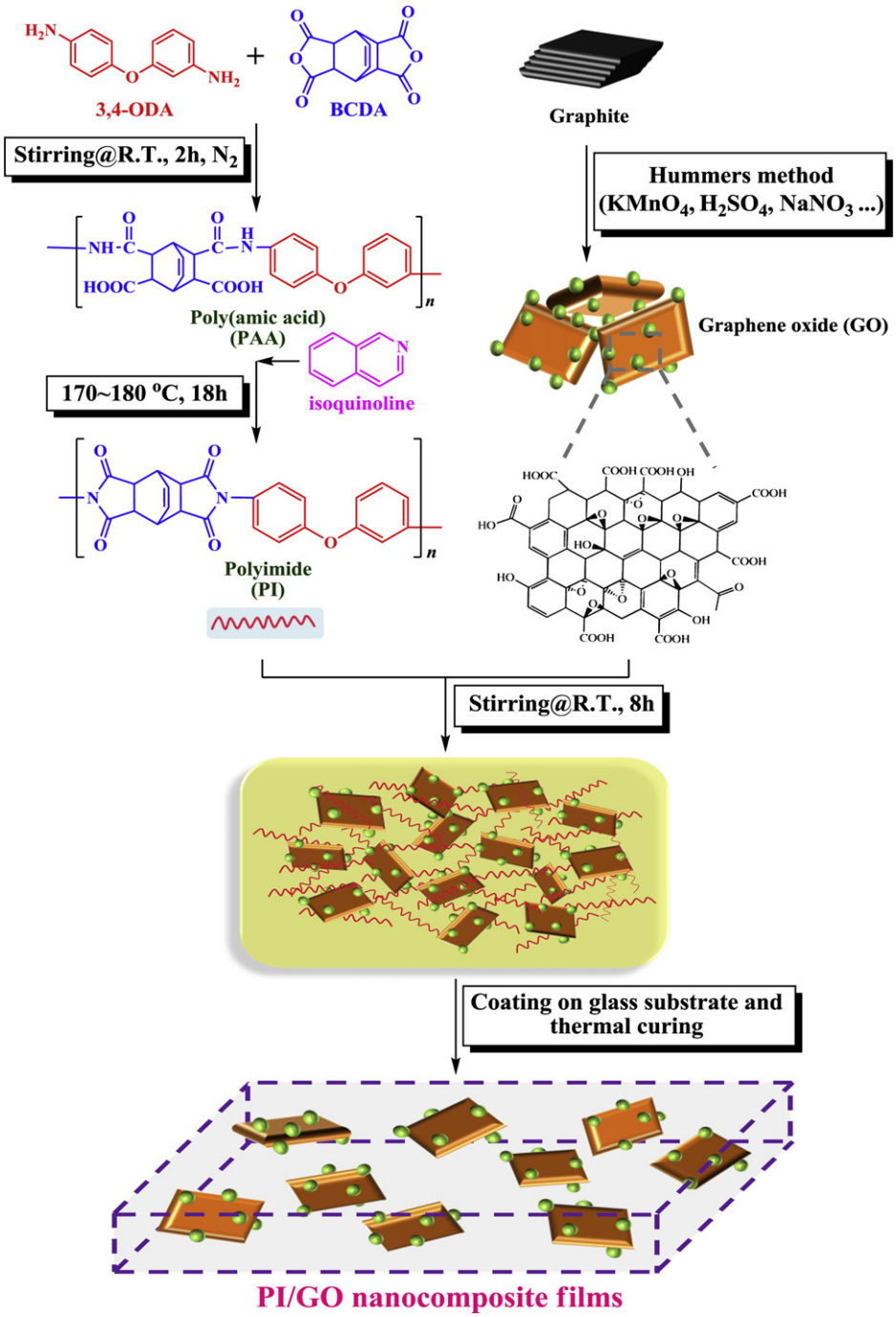

Scheme 1. Synthesis process of PI/GO nanocomposite films.

morphology [37–40] were observed from the TEM image (Fig. 1(a)) of synthesized GO sample compared with the heavily stacked graphic layers of graphite flakes, *i.e.* GO precursor. The XRD pattern of natural graphite shown in Fig. 1(b) revealed the characteristic intense refraction peak of graphite at $2\theta = 26.4°$, which corresponds to the graphene interlayer of (002) with the d spacing of 0.34 nm [39,41,42]. After the oxidation process by modified Hummers method, dried GO had a weak diffraction peak at $2\theta = 9.7°$. The disappearance of the characteristic graphite peak at 26.4° and the formation of a weak peak at 9.7° ($d = 0.92$ nm) indicated the intercalation of hydroxyl, carbonyl and epoxide groups in graphite interlayer during the chemical oxidation process [28,41–43]. Those functional groups on the surface of GO as confirmed in our previous study were beneficial for the dispersion of GO in PAA or PI solution. In this study, the GO loading was limited to 0.01 wt% in order to maintain high optical transparency of PI film. However, the distribution of GO in PI samples containing GO less than 0.01 wt% was difficult to be directly resolved by SEM or TEM images. Hence, Fig. 1(c) and (d) were the SEM images of cross section of PI/GO-0.01 nanocomposite. Highly wrinkled GO nanosheets were distributed in PI matrix and some GO aggregation was observed at this highest GO loading.

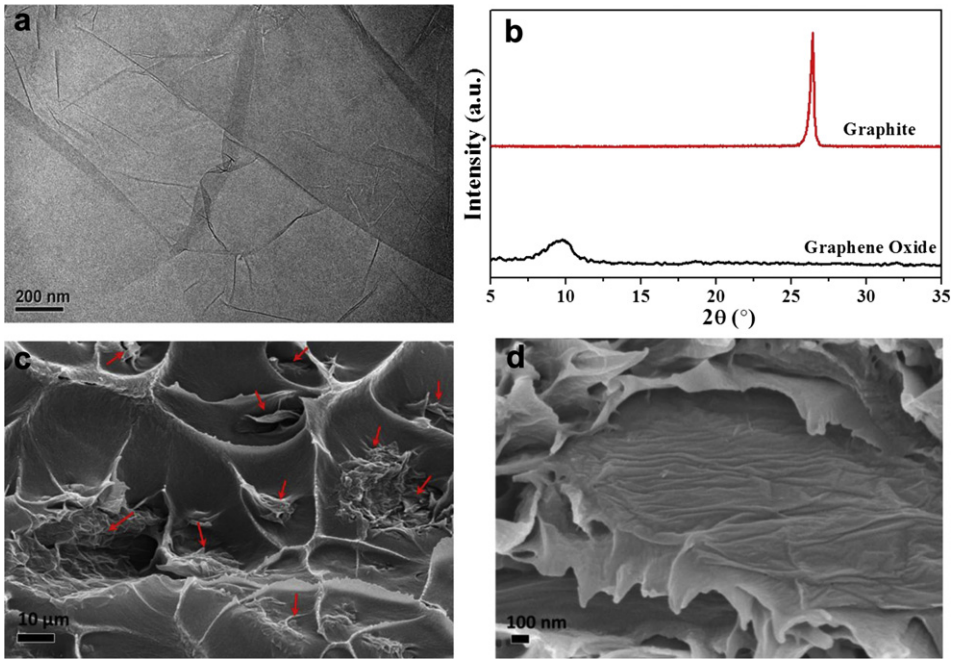

Fig. 1. (a) TEM image of dried GO; (b) XRD patterns of graphite and dried GO; (c) SEM image of cross section of PI/GO-0.01 nanocomposite film. The arrows indicate the dispersed GO in PI matrix. (d) The magnified image of GO from the cross section of PI/GO-0.01 nanocomposite film.

3.2. Imidization degree of PI

In this study, the organo-soluble PI was synthesized via one-step method. The obtained PI solution was mixed with KBr in order to conduct the variable-temperature FTIR measurements to determine the imidization degree of PI. As shown in Fig. 2, the characteristic imide absorption bands at 715 cm^{-1} (C═O bending), 1380 cm^{-1} (C–N stretching), 1716 and 1774 cm^{-1} (symmetrical and asymmetrical C═O stretching) [10,44] were presented on the IR spectrum of PI sample as the temperature reached 140 °C. The characteristic imide absorption band at 715 cm^{-1} was chosen to estimate the imidization degree of PI precursors at different temperatures because there is less interference from the anhydride, catalyst and solvent functional groups in this frequency range. An internal standard at the frequency of 1500 cm^{-1} (C═C stretching in benzyl ring group) was selected to normalize the intensity of the above peak and hence to eliminate the effect of film thickness on the resultant intensity. That is, the imidization degree at a specific temperature (T) was determined from the ratio of relative intensity (*i.e.* peak area) of absorption bands at a specific temperature $(A_{715}/A_{1500})_T$ to that at 300 °C $(A_{715}/A_{1500})_{300}$, where completely imidization was assumed occurred. The imidization degree gradually increased from 89 to 92% with the reaction temperature elevating from 180 to 280 °C. Consequently, the imidization degree of the casted film was estimated higher than 90%.

3.3. Optical transparency of pure PI and PI/GO nanocomposites

The selection of alicyclic BCDA and asymmetric ODA in the cosolvent of DMAc and GBL successfully fabricated flexible colorless PI film. The transmission UV–Vis spectra of pure PI films with various thicknesses were shown in Fig. 3. The pure PI with the standard practical thickness (25 μm) illustrated the transmittance higher than 85% in the whole visible light region. The transmittance increased with the decreasing film thickness. For pure PI with the thickness less than 3 μm, the optical transmittance in the visible light region (400–800 nm) was higher than 90%. The high optical transparency was because of the polyalicylic unit in the polymer

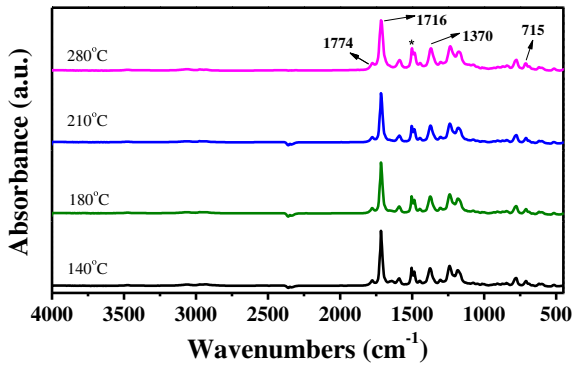

Fig. 2. Variable-temperature FTIR spectra of pure PI solution spin-coated on KBr.

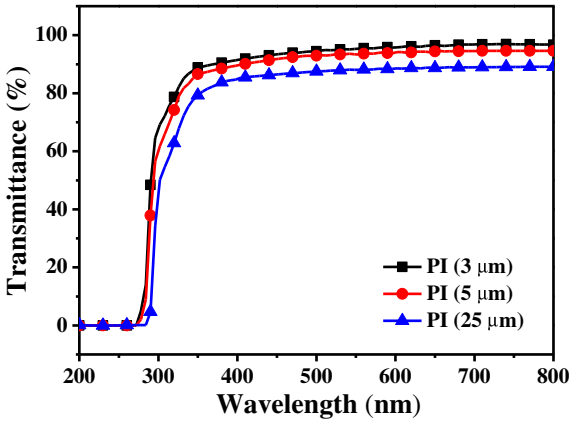

Fig. 3. UV–Vis spectra of pure PI films with various thicknesses.

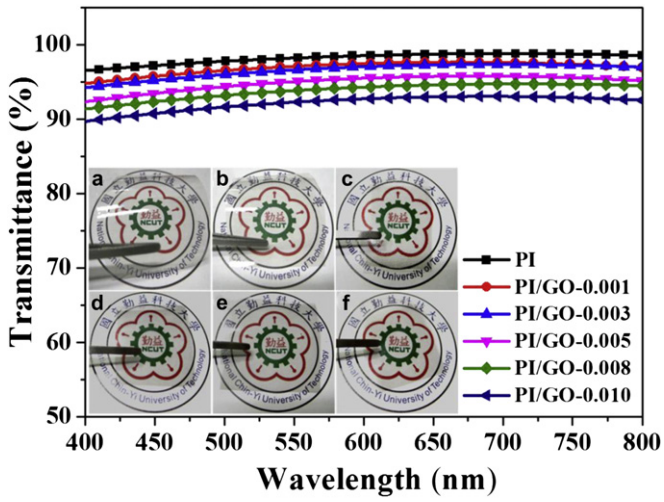

Fig. 4. UV–Vis spectra in the visible light region of pure PI and PI/GO nanocomposite films (same thickness: 2 μm) with various GO contents. *Inset*: The digital photographs of (a) pure PI, (b) PI/GO-0.001, (c) PI/GO-0.003, (d) PI/GO-0.005, (e) PI/GO-0.008, and (f) PI/GO-0.010 nanocomposite films.

chain [45,46]. Matsumoto and Kurosaki [45] reported a comparable optical transparency of 94% for PI film with a thickness of 12 μm by selecting from similar monomers. However, two-step polymerization was required to obtain PIs with sufficient mechanical strength.

The digital photograph of nearly colorless PI was shown in the inset of Fig. 4 as well as those of PI/GO nanocomposite films. With the incorporation of GO in PI matrix, the optical transparency slightly decreased with the content of GO. Fig. 4 illustrated the transmittance of PI and PI/GO films with the thickness of 2 μm in the visible light region. For the highest loading of GO in this work, *i.e.* 0.01 wt%, the transmittance at 550 nm was 91% for PI/GO-0.010 film, compared with 97% for pure PI. Liaw et al. [10] also reported a fluorinated PI film with a thickness of 5 μm exhibited the transmittance at 500 nm of 97% and the transmittance decreased with the content of nanoparticles in PI matrix. Hence, in this study, the GO content was limited to only 0.01 wt% to remain sufficient optical transmittance of PI for practical applications. Furthermore, the yellowness index, *i.e.* b^* value, of each synthesized film was very small ranging from 0.6 to 0.9 as listed in Table 1. Those results suggested the obtained PI/GO nanocomposites were nearly colorless and had excellent optical transparency and clarity. The alicyclic structure of BCDA and flexible ether linkage of ODA resulted in less conjugated structure in PI matrix and thus reduced the absorption of visible lights and the formation of inter- or intra-molecular charge transfer complex between or within polymer backbones [7,45,46]. In addition, the surface functional groups of ultra thin GO facilitated the uniform dispersion of GO in DMAc and in PI solution with the assistance of ultrasonication. Hence, the optical transparency of PI/GO was still high and some properties, especially the barrier property, of PI/GO were improved.

Table 1
Optical properties of pure PI and PI/GO hybrid films.[a]

Sample	UV–Vis		Color meter			
	T_{400nm}[b] (%)	T_{550nm}[c] (%)	Haze (%)	L^*	a^*	b^*
Pure PI	96	97	0.2	96.08	−0.23	0.63
PI/GO-0.001	95	97	0.6	95.70	−0.27	0.79
PI/GO-0.003	94	95	0.5	95.49	−0.25	0.82
PI/GO-0.005	92	94	1.1	95.10	−0.25	0.92
PI/GO-0.008	90	93	1.0	94.65	−0.15	0.81
PI/GO-0.010	89	91	1.6	94.25	−0.21	0.86

[a] Films with the thickness of around 2 μm.
[b] Transmittance at 400 nm.
[c] Transmittance at 550 nm.

3.4. Gas barrier property of PI/GO nanocomposites

The effect of GO content on WVTR of films was shown in Fig. 5. A significant decrease in WVTR, from 181 to 31 g mil m^{-2} day^{-1}, was observed upon the addition of 0.001 wt% of GO in PI matrix. The WVTR of PI/GO-0.001 was only 17% of that of pure PI and then gradually decreased with the increasing GO content to 0.01 wt%. The distribution of GO with the features of high aspect ratio and high specific surface area in PI matrix can effectively extend the path of the water vapor passing through the thin film [19,27,28] and thus significantly improved water vapor barrier property.

3.5. Mechanical strength and thermal stability and of PI/GO nanocomposites

The DMA results of pure PI and PI/GO nanocomposites were shown in Fig. 6 and summarized in Table 2. The storage modulus (E') of hybrid films increased remarkably with the increase of GO contents. The E' value at 60 °C was 1487 MPa for pure PI and increased to 2474 MPa for PI hybrids containing 0.01 wt% GO. The reinforcement effect from GO was mainly attributed to its fine dispersion and high orientation in PI matrix, as well as the efficient load transfer from the matrix to GO nanosheets, and thus significantly enhanced the mechanical strength of nanocomposite.

The glass transition temperature (Tg) determined from the peak of tan delta curve of each sample was listed in Table 2. The negligible variation in Tg values with GO content indicated similar stiffness of PI chains in each film. The one-step process applied to synthesize PI had almost completed the imidization reaction that few amino and/or carboxyl groups on PI remained in PI matrix to form the bonding with GO. The chain–chain interaction between GO and PI matrix was weak that GO provided less restriction of movement from PI main chains. Therefore, the presence of GO did not change the imidization degree or the chain length of synthesized PI that the Tg values of PI and PI/GO were all around 350 °C.

High dimensional stability is one important feature for PI-based nanocomposites as they are potentially used in flexible printed

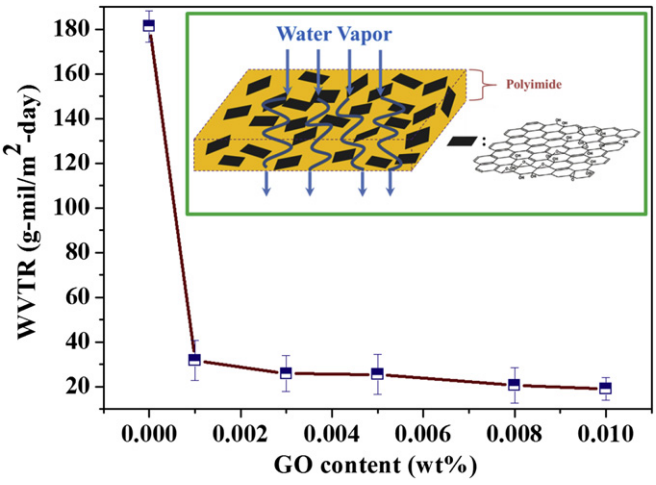

Fig. 5. Effect of GO contents on the water-vapor-transmission-rate (WVTR) of pure PI and PI/GO nanocomposite films. Note: WVTR was measured at 40 °C and 100% RH. *Inset*: Illustration of water barrier property of PI/GO nanocomposite film.

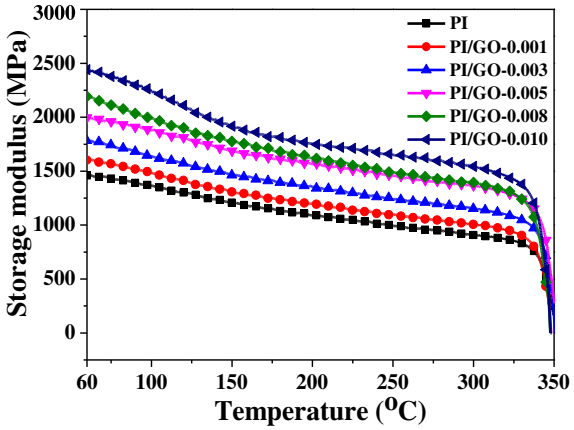

Fig. 6. The storage modulus curves of pure PI and PI/GO nanocomposite films.

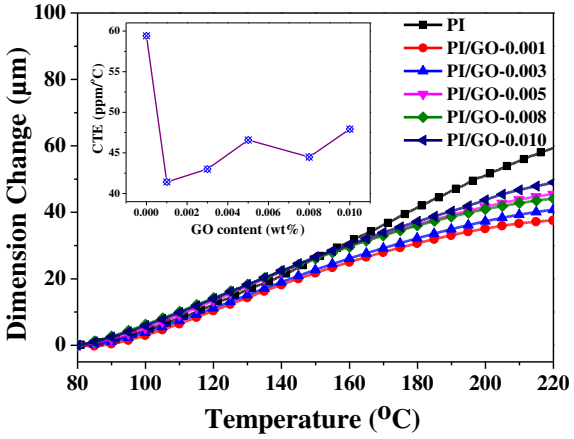

Fig. 7. TMA curves of pure PI and PI/GO nanocomposite films. *Inset*: Effect of GO content on the coefficient of thermal expansion (CTE) in the temperature range of 100–200 °C.

circuits (FPCs) to laminate with copper. The CTEs determined from the TMA results (Fig. 7) in the range of 100–200 °C were listed in Table 2. The incorporation of GO remarkably decreased the CTE of PI nanocomposites. The lowest CTE obtained in the study was 41 ppm $°C^{-1}$ for PI/GO-0.001 and compared with 59 ppm $°C^{-1}$ for pure PI. The addition of those nearly one-dimensional GO nanosheets is believed to enhance the chain orientation of PI and thus resulting to lower CTE [47]. In addition, the homogeneous dispersion of ultra thin GO nanosheets in PI matrix decreased the free volume in PI matrix and consequently reduced the CTE of nanocomposites. As shown in the inset of Fig. 7, the CTE of PI/GO nanocomposites with GO loading from 0.001 to 0.01 wt% slightly increased with GO content. Continuous increase in GO loading might lead to some aggregation of GO in PI matrix that the free volume in PI matrix might be slightly enlarged, as shown in Fig. 1(c) and (d) for the morphology of PI/GO-0.01, and thus CTE was increased.

The TGA results of pure PI and PI/GO nanocomposites are demonstrated in Fig. 8. The thermal decomposition temperature (Td) at 5% weight loss of PI/GO was decreased with the content of GO. It is believed that the easily decomposed carboxyl or hydroxyl groups on GO might accelerate the degradation of PI and thus decline the thermal stability of PI matrix [41]. Despite the decrease in Td, the Td value of PI/GO-0.001 retains higher than 400 °C, compared with 427 °C for pure PI, indicating sufficient thermal stability of obtained PI/GO nanocomposites for practical applications.

Table 2
Physical, mechanical and thermal properties of pure PI and PI/GO nanocomposite films.

Sample	Thickness (μm)	DMA		TMA	TGA	WVTR[e]
		E'[a] (MPa)	Tg[b] (°C)	CTE[c] (ppm $°C^{-1}$)	Td_5[d] (°C)	(g mil m^{-2} day^{-1})
Pure PI	18	1487	349	59	427	181
PI/GO-0.001	20	1637	347	41	422	32
PI/GO-0.003	19	1811	349	43	423	26
PI/GO-0.005	21	2047	348	46	419	26
PI/GO-0.008	18	2251	347	45	407	21
PI/GO-0.010	17	2474	347	48	408	19

[a] Storage modulus at 60 °C.
[b] The temperature at the maximum of tan δ curve was designated as Tg.
[c] The coefficient of thermal expansion (CTE) determined over the range of 100–200 °C.
[d] The thermal decomposition temperature at 5% weight loss.
[e] Water-vapor-transmission-rate (WVTR) at 40 °C and 100% RH.

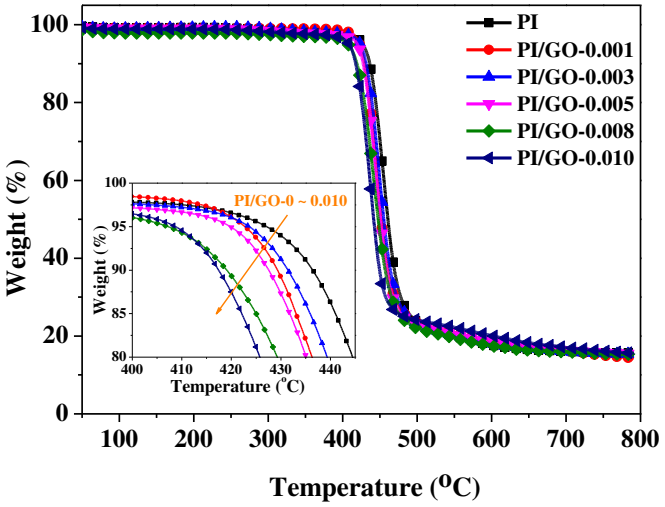

Fig. 8. TGA curves of pure PI and PI/GO nanocomposite films. *Inset*: TGA curves in the temperature range of 400–445 °C.

4. Conclusions

In this study, we have successfully prepared transparent and colorless PI films by using alicyclic dianhydride and asymmetric diamine monomers via one-step process. With the incorporation of ultra thin GO nanosheets in PI, the resultant PI/GO nanocomposites remain excellent optical transmittance and have enhanced mechanical strength and dimensional stability. Most importantly, GO forms a moisture barrier that the PI/GO nanocomposite exhibits improved resistance to water vapor. With the addition of only 0.001 wt% of GO, a dramatic reduction (83%) in the moisture permeability rate was observed for the resultant PI nanocomposite (PI/GO-0.001). The PI/GO-0.001 nanocomposite exhibits the transmittance in the visible light range higher than 95% and the lowest CTE, 41 ppm $°C^{-1}$, together with sufficient thermal stability. The results suggest the synthesized PI/GO nanocomposites are potential candidates for the applications, such as the substrates of advanced touch panel or flexible display, where high optical transparency and good water resistance are essentially required.

Acknowledgments

The authors would like to acknowledge the financial support from the Ministry of Economic Affairs, Taiwan, through the project on flexible polymeric materials for electronic application (100-EC-17-A-07-S1-120).

References

[1] T. Hasegawa, K. Horie, Prog. Polym. Sci. 26 (2001) 259.
[2] Y.N. Sazanov, Russ. J. Appl. Chem. 74 (2001) 1253.
[3] J.J. Ge, D. Zhang, Q. Li, H.Q. Hou, M.J. Graham, L.M. Dai, F.W. Harris, S.Z.D. Cheng, J. Am. Chem. Soc. 127 (2005) 9984.
[4] Y.Z. Bin, K. Oishi, A. Koganemaru, D. Zhu, M. Matsuo, Carbon 43 (2005) 1617.
[5] J.G. Liu, Y. Nakamura, Y. Suzuki, Y. Shibasaki, S. Ando, M. Ueda, Macromolecules 40 (2007) 7902.
[6] J.G. Liu, Y. Nakamura, Y. Shibasaki, S. Ando, M. Ueda, Macromolecules 40 (2007) 4614.
[7] S.H. Hsiao, C.P. Yang, H.S. Chen, J. Polym. Sci. A Polym. Chem. 38 (2000) 1551.
[8] R.E. Southward, D.S. Thompson, T.A. Thornton, D.W. Thompson, A.K. Clair St, Chem. Mater. 10 (1998) 486.
[9] H.S. Jin, J.H. Chang, J.C. Kim, Macromol. Res. 16 (2008) 503.
[10] W.C. Liaw, Y.L. Cheng, Y.S. Liao, C.S. Chen, S.M. Lai, Polym. J. 43 (2011) 249.
[11] Y.W. Wang, W.C. Chen, Compos. Sci. Technol. 70 (2010) 769.
[12] T. Lee, S.S. Park, Y.I. Jung, S. Han, D. Han, I. Kim, C.S. Ha, Eur. Polym. J. 45 (2009) 19.
[13] J.C. Tang, G.L. Lin, H.C. Yang, G.J. Jiang, Y.W. Chen-Yang, J. Appl. Polym. Sci. 104 (2007) 4096.
[14] J.S. Park, J.H. Chang, Polym. Eng. Sci. 49 (2009) 1357.
[15] J.H. Park, J.H. Kim, J.W. Park, J.H. Chang, C.S. Ha, J. Nanosci. Nanotechnol. 8 (2008) 1700.
[16] U. Min, J.H. Chang, J. Nanosci. Nanotechnol. 11 (2011) 6404.
[17] H.Y. Huang, T.C. Huang, T.C. Yeh, C.Y. Tsai, C.L. Lai, M.H. Tsai, J.M. Yeh, Y.C. Chou, Polymer 52 (2011) 2391.
[18] T.C. Huang, C.F. Hsieh, T.C. Yeh, C.L. Lai, M.H. Tsai, J.M. Yeh, J. Appl. Polym. Sci. 119 (2011) 548.
[19] O.C. Compton, S. Kim, C. Pierre, J.M. Torkelson, S.T. Nguyen, Adv. Mater. 22 (2010) 4759.
[20] J.R. McBride, A.R. Lupini, M.A. Schreuder, N.J. Smith, S.J. Pennycook, S.J. Rosenthal, ACS Appl. Mater. Interfaces 1 (2009) 2886.
[21] R. Verdejo, F. Barroso-Bujans, M.A. Rodriguez-Perez, J.A. De Saja, M.A. Lopez-Manchado, J. Mater. Chem. 18 (2008) 2221.
[22] H.C. Schniepp, J.L. Li, M.J. McAllister, H. Sai, M. Herrera-Alonso, D.H. Adamson, R.K. Prudhomme, R. Car, D.A. Saville, I.A. Aksay, J. Phys. Chem. B 110 (2006) 8535.
[23] S. Ansari, E.P. Giannelis, J. Polym. Sci. B Polym. Phys. 47 (2009) 888.
[24] J.S. Bunch, S.S. Verbridge, J.S. Alden, A.M. van der Zande, J.M. Parpia, H.G. Craighead, P.L. McEuen, Nano Lett. 8 (2008) 2458.
[25] S. Stankovich, D.A. Dikin, G.H.B. Dommett, K.M. Kohlhaas, E.J. Zimney, E.A. Stach, R.D. Piner, S.T. Nguyen, R.S. Ruoff, Nature 442 (2006) 282.
[26] J.R. Potts, D.R. Dreyer, C.W. Bielawski, R.S. Ruoff, Polymer 52 (2011) 5.
[27] H. Kim, Y. Miura, C.W. Macosko, Chem. Mater. 22 (2010) 3441.
[28] H.M. Kim, J.K. Lee, H.S. Lee, Thin Solid Films 519 (2011) 7766.
[29] J.H. Yeun, G.S. Bang, B.J. Park, S.K. Ham, J.H. Chang, J. Appl. Polym. Sci. 101 (2006) 591.
[30] J. Jang, D.K. Lee, Polymer 45 (2004) 1599.
[31] D. Feldman, J. Polym. Environ. 9 (2001) 49.
[32] M. Salame, S. Steingiser, Polym. Plast. Technol. Eng. 8 (1977) 155.
[33] N.I. Kovtyukhova, P.J. Ollivier, B.R. Martin, T.E. Mallouk, S.A. Chizhik, E.C. Buzaneva, A.D. Gorchinskiy, Chem. Mater. 11 (1999) 771.
[34] J.K. Lee, K.B. Smith, C.M. Hayner, H.H. Kung, Chem. Commun. 46 (2010) 2025.
[35] D.C. Marcano, D. Kosynkin, J.M. Berlin, A. Sinitskii, Z. Sun, A. Slesarev, L.B. Alemany, W. Lu, J.M. Tour, ACS Nano 4 (2010) 4806.
[36] W.S. Hummers Jr., R.E. Offeman, J. Am. Chem. Soc. 80 (1958) 1339.
[37] Y.W. Zhu, S. Murali, W.W. Cai, X.S. Li, J.W. Suk, J.R. Potts, R.S. Ruoff, Adv. Mater. 22 (2010) 3906.
[38] J.Y. Wang, S.Y. Yang, Y.L. Huang, H.W. Tien, W.K. Chin, C.C.M. Ma, J. Mater. Chem. 21 (2011) 13569.
[39] N.D. Luong, N. Pahimanolis, U. Hippi, J.T. Korhonen, J. Ruokolainen, L.S. Johansson, J.D. Nam, J. Seppala, J. Mater. Chem. 21 (2011) 13991.
[40] B. Shen, W.T. Zhai, C. Chen, D.D. Lu, J. Wang, W.G. Zheng, ACS Appl. Mater. Interfaces 3 (2011) 3103.
[41] D. Chen, H. Zhu, T.X. Liu, ACS Appl. Mater. Interfaces 2 (2010) 3702.
[42] G.X. Wang, J. Yang, J. Park, X.L. Gou, B. Wang, H. Liu, J. Yao, J. Phys. Chem. C 112 (2008) 8192.
[43] Y. Xu, W. Hong, H. Bai, C. Li, G. Shi, Carbon 47 (2009) 3538.
[44] T. Matsumoto, Macromolecules 32 (1999) 4933.
[45] T. Matsumoto, T. Kurosaki, Macromolecules 30 (1997) 993.
[46] C.P. Yang, S.H. Hsiao, C.H. Chen, Polym. J. 29 (1997) 944.
[47] S. Ebisawa, J. Ishii, M. Sato, L. Vladimirov, M. Hasegawa, Euro. Polym. J. 46 (2010) 283.